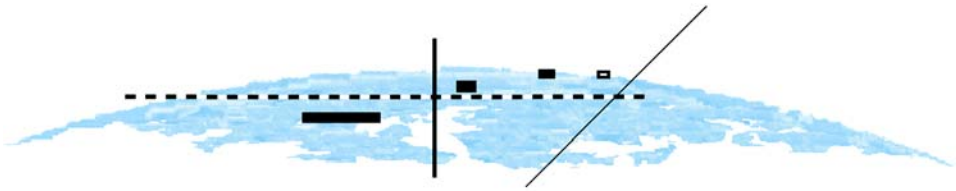

GeoForschungsZentrum Potsdam

STIFTUNG DES ÖFFENTLICHEN RECHTS

Scientific Technical Report

ISSN 1610-0956

Geostrophic Ocean Surface Velocities from TOPEX Altimetry, and CHAMP and GRACE Satellite Gravity Models

Henryk Dobslaw [1,2], Peter Schwintzer [1], Franz Barthelmes [1], Frank Flechtner [1], Christoph Reigber [1], Roland Schmidt [1], Tilo Schöne [1], Martin Wiehl [2]

[1] GeoForschungsZentrum Potsdam (GFZ), Department 1, Telegrafenberg, 14473 Potsdam

[2] Institut für Planetare Geodäsie, Technische Universität Dresden, Mommsenstraße 13, 01062 Dresden

Abstract

Recently released global gravity field models generated solely from CHAMP and GRACE satellite observations allow with an unprecedented accuracy and resolution the recovery of the mean sea surface topography from the difference between an altimetry-based mean sea surface height model and the gravity model's derived geoid. Here the CHAMP EIGEN-2 gravity field model, and the first GFZ GRACE gravity model, EIGEN-GRACE01S, are used. The mean sea surface height model has been compiled from four years' worth of TOPEX altimeter data. To evaluate the accuracy and resolution limits of the CHAMP and GRACE geoids for the envisaged application, a low pass filter in the spatial domain with different cut-off wavelengths has been applied to the geoid and sea surface data before subtraction. The minimum wavelength, where noisy and erroneous features in the recovered sea surface topography are minimised, can be interpreted as an indicator for the best suited common spatial resolution. The EIGEN-2 model's geoid has been tested to have a resolution of 1800 km, which corresponds to a truncation degree of l = 22 in terms of spherical harmonics. Using the EIGEN-GRACE01S model, the resolution could be extended to 1000 km (l = 40). These boundaries can be attributed to the geoid's error, exceeding 2 cm in case of the CHAMP model, and in case of the GRACE model to spurious systematic signals increasing with increasing spherical harmonic degree. The calculated sea surface topography models have been used to derive absolute geostrophic sea surface velocities. An error propagation shows that the requirement of 1 cm/s for geoid induced velocity errors is fulfilled at the given resolutions for all latitudes excluding a narrow equatorial band. Maximum geostrophic velocities are derived in the 1000 km-resolution model for the Kuroshio region with 40 cm/s, and for the Gulf Stream east off Cape Hatteras with 25 cm/s.

Keywords: global gravity field models, mean sea surface, sea surface topography, geostrophic ocean surface currents

1 Introduction

Beside the equatorial region, ocean currents are very close to the geostrophic balance on time scales longer than a few days. Therefore, the dynamic ocean topography, i.e., the deviation of the stationary sea surface from the marine geoid, is a direct measure of the dynamic pressure at the sea surface which leads to the geostrophic part of the surface current velocity.

The determination of the general ocean circulation has been a longstanding problem in physical oceanography. Wunsch and Gaposchkin [1980] gave already in 1980 a comprehensive view of the problems that have to be solved to reach this ambitious goal. Over the years altimetric measurements of the sea surface as well as modelling skills have been greatly improved (see the extensive review by Wunsch and Stammer [1998]), but the accuracy of the geoid models still has been inferior to the quality of the altimetric models [Fu and Chelton, 2001].

Accordingly, previously published dynamic ocean topography models suffered mainly from the poor quality of the marine geoid when derived solely from satellite tracking data, or were biased when using altimetric measurements for geoid determination [Le Traon et al., 2001]. With the advent of the first models from the new dedicated gravity missions CHAMP and GRACE the quality of the gravity field models based on satellite tracking data significantly increased [Reigber et al., 2003a, Reigber et al., 2003b]. Consequently ocean topography derived from these models should give more detailed information about the steady ocean circulation than before. First insights have been given by Gruber and Steigenberger [2002], and Tapley et al. [2003]. According to fundamentally different kinds of the underlying measurements, i.e., point-wise sampling of the sea surface with satellite altimetry vs. satellite orbit perturbation analysis, sea surface and geoid models have considerably different spatial resolutions. To compare both models it is necessary to accommodate the resolution of both fields. This is done here in the spatial domain by applying a moving average filter.

The gain in accuracy and resolution using the recently released gravity field models generated from CHAMP and GRACE data for calculating sea surface topography will become obvious. From the resulting sea surface topography models the corresponding geostrophic velocities

are derived and some general ocean circulation features are discussed that now are detectable from space.

2 Satellite Gravity Field Models

The EIGEN-2 global gravity field model [Reigber et al., 2003a], represented by the coefficients of a spherical harmonic expansion of the gravitational potential, is derived solely from CHAMP GPS satellite-to-satellite tracking and accelerometer data that cover an observation period of seven months out of the years 2000 and 2001. The EIGEN-GRACE01S global gravity field model [Reigber et al., 2003b] is the first GRACE solution, computed at GeoForschungsZentrum Potsdam (GFZ), and derived from only 39 days' (out of August and November 2002) worth of GRACE GPS satellite-to-satellite tracking, accelerometer and K-band low-low satellite-to-satellite tracking data.

Figure 1 depicts, in terms of geoid heights, the signal amplitudes per degree of the spherical harmonic coefficients of both solutions. It can be seen that with the CHAMP configuration the resolution of the gravity field is restricted in the EIGEN-2 model to about degree/order 40 (1000 km wavelength at the Earth's surface) due to signal attenuation for higher degree terms. Thanks to the precise low-low ranging capability, the dual-satellite mission GRACE fully resolves the gravitational signal almost up to degree/order 100 (400 km wavelength at the Earth's surface). Also, the GRACE solution is over a wide range of the solved-for gravitational spectrum about one to two orders of magnitude more accurate than the CHAMP solution as can be seen from Figures 1 and 2, where the geoid error amplitudes per degree and accumulated as a function of maximum degree, respectively, are given.

It can be deduced from Figure 2 that the 2 cm threshold, which is supposed to be the required geoid accuracy for the application envisaged in this study, is exceeded at degree 22 with the EIGEN-2 derived geoid and only at degree 68 with the EIGEN-GRACE01S model. For the CHAMP model, this limitation is verified by the amplitudes of the differences between the CHAMP and GRACE models as a function of maximum degree, also shown in Figure 2. The accuracy estimates for both models result from the formal errors as obtained in the least-squares adjustment of the spherical harmonic coefficients. The formal errors were then a posteriori calibrated using the scattering of sub-set solutions from independent data periods. The application of both gravity field models in sea surface topography recovery will indicate whether the error calibration has been done properly.

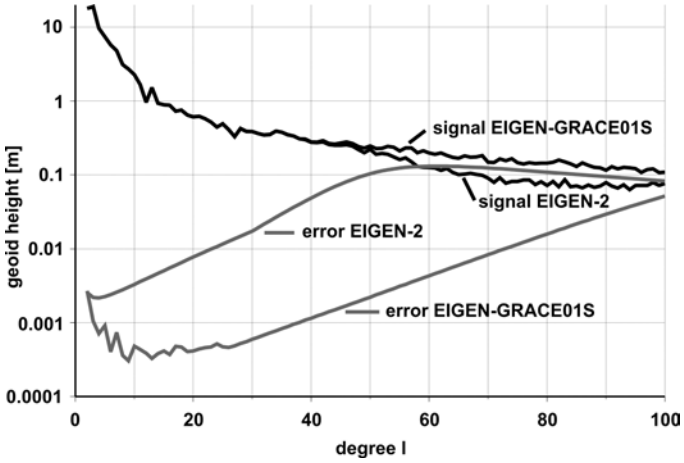

Figure 1. Signal amplitudes and error estimates per degree of the spherical harmonic coefficients from EIGEN-2 and EIGEN-GRACE01S.

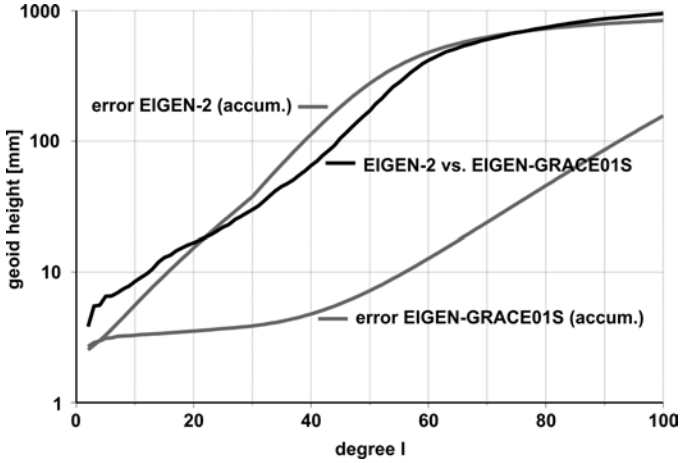

Figure 2. Geoid errors as a function of maximum degree of EIGEN-2 and EIGEN-GRACE01S as well as differences as a function of maximum degree between EIGEN-2 and EIGEN-GRACE01S in terms of geoid heights.

3 Mean Sea Surface Height Model

Mean sea surface height (MSSH) models provide the basis for the calculation of sea surface topography, i.e. the difference between the time averaged sea surface and the geoid. In recent years several MSSH models have been published, e.g. CLS01 [Hernandez and Schaeffer, 2001] or GSFC00.1 [Wang, 2001]. These models are computed using data from different altimeter satellites with different orbit repeat periods and inclinations, and covering different time periods in order to achieve a small data spacing and a long-term temporal averaging. But, the signal averaging period, which has to be known for ocean circulation models, is not exactly defined because of the missions' data combination. Here, the MSSH model will be

used together with satellite-only gravity fields that are derived from data taken only since the launch of the CHAMP satellite in the year 2000 [Reigber et al., 2002]. Thus, a MSSH model is needed with a time span very close to this period to avoid signals resulting from the long-term trend of the mean sea surface.

During recent years the Altimeter Database and Processing System (ADS, gesis.gfz-potsdam.de/ads) was developed providing state-of-the-art altimeter data from various missions as well as a wide range of processing tools to users. All altimeter data are upgraded for known deficiencies, and the system provides a number of geophysical correction models. Using ADS, a MSSH model was computed covering four years of data (05/01/1998 through 05/01/2002). Taking the full 4-years period averages seasonal variations, caused for instance by thermal expansion. In addition, the effect of the peak period of the El Niño event around 1997/1998 is avoided.

Only TOPEX [NASA, 1992] data are used, computed using the NASA orbit based on the JGM-3 gravity field, the GOT02.2 ocean tide and loading model [Ray, 1999] and DORIS micro-wave tracking measurements to correct the ionospheric pass delay. The tropospheric attenuation is corrected using radiometer data for the wet and ECMWF (European Center for Medium Range Weather Forecast) data for the dry troposphere. Solid Earth tides have been corrected applying the model of Cartwright and Tayler [1971] and Cartwright and Edden [1973]. In addition, the pole tide was corrected [Wahr, 1985] using the polar motion series EOP-C04 from the International Earth Rotation and Reference System Service (IERS).

Various editing criteria have been tested in order to find a compromise between outlier rejection and the number of useful data. All valid measurements within a radius of three degrees have been interpolated onto a regular grid with a spacing of 0.25 deg. Finally the resulting MSSH model was reduced from the mean-tide to a tide-free system [Rapp et al., 1991].

A comparison with the GSFC00.1 MSSH model shows a root mean square (rms) of the differences of 6.8 cm globally. These values fit quite well to the ones estimated by Hernandez and Schaeffer [2000], comparing various MSSH models with rms values of the differences between 6 and 10 cm. Additionally, a comparison of 6 years TOPEX mean tracks to a one year average carried out by Wang [2001] gave an rms of 6.4 cm. This value has been interpreted most likely to represent time variations of the sea surface height.

Typical measurement errors of TOPEX can be reduced to less than 1 cm on spatial scales larger than 100 km [Chelton et al., 2001]. Other major sources of errors are corrections for

atmospheric refraction as well as sea state and time bias. The overall effect of these effects has been estimated to be 2.7 cm [Chelton et al., 2001]. Additionally, the error impact of the quality of the underlying JGM-3 orbit has been calculated to be approximately 2.5 cm [Ries and Tapley, 1999]. Whereas the first-mentioned errors are mostly stochastically distributed and therefore will reduce during long-time averaging, the geographically correlated orbit errors can not be reduced this way. For the wavelengths longer than 1000 km, which are of interest here, the accuracy of the MSSH model is eventually estimated to be 2 cm.

4 Linear Filtering

Gravity field models and altimetry-based sea surface height models considerably differ in spatial resolution. Gravity field models based on satellite tracking data only do not contain as much small scale information as altimetry data do. Different approaches have been presented to fade out the high frequency signal parts in the sea surface height models: Gruber and Steigenberger [2002], and Tapley et al. [2003] used filtering in the spherical harmonics domain for calculating dynamic ocean topography from altimetry with respect to the CHAMP-based EIGEN-1S geoid [Reigber et al., 2002] and the American GRACE-based GGM01 geoid [UTEX/CSR, 2003], respectively. For a global coverage, the continental and polar gaps of the altimetric surface had been filled with geoid heights from EGM96 [Lemoine et al., 1998]. Rapp et al. [1996] point out that such a representation can produce power spectra that are not truly representative. They suggest using a set of functions that are orthonormal over the oceans, but the construction of the orthonormal functions depends on the area covered by the observations. Here, the accommodation of the spatial resolutions in both the geoid and the MSSH model will be done via a moving average filter directly in the spatial domain.

Applying a low pass filter to both models enables to damp the high frequency signals, which are poor determined in the gravity field model and to fit the sea surface height model to the meaningful resolution triggered by the accuracy of the geoid model. Thereby, one must be careful not to wipe out significant parts of the oceanic signal. The limiting wavelength representing the best compromise can be regarded as a realistic indicator for the spatial resolution of the gravity field model given a certain accuracy level.

Table 1. Definition of different impulse responses for moving weighted average low pass filters. The distance r is given in units of filterwidth.

Rectangle	$g_r = \begin{cases} 1 & \lvert r \rvert \le 0.5 \\ 0 & \lvert r \rvert > 0.5 \end{cases}$
Triangle	$g_r = \begin{cases} 1-2r & \lvert r \rvert \le 0.5 \\ 0 & \lvert r \rvert > 0.5 \end{cases}$
Hanning	$g_r = \begin{cases} \dfrac{1+\cos 2\pi r}{2} & \lvert r \rvert \le 0.5 \\ 0 & \lvert r \rvert > 0.5 \end{cases}$
Gauss	$g_r = \begin{cases} e^{-\frac{1}{2}(6r)^2} & \lvert r \rvert \le 0.5 \\ 0 & \lvert r \rvert > 0.5 \end{cases}$
Hamming	$g_r = \begin{cases} 0.535 + 0.465\cos 2\pi r & \lvert r \rvert \le 0.5 \\ 0 & \lvert r \rvert > 0.5 \end{cases}$

To find out the optimum filter design, different impulse responses have been tested (Table 1). Due to rotational symmetry of the two-dimensional impulse responses, the corresponding transfer functions can be calculated through a one-dimensional Hankel-Transform:

$$G(\nu) = \int_0^\infty g(r) J_0(2\pi\nu r) r dr \qquad (1)$$

$G(\nu)$ is the transfer function depending on the frequency ν, $g(r)$ is the impulse response as a function of the spherical distance r given in units of wavelength, and $J_0(2\pi\nu r)$ is the Bessel function of the first kind. The goal is to construct a low pass filter, which leaves those signals with frequencies lower than the cut-off frequency undeformed and fades out the higher frequencies. Additionally, the filter width, i.e. twice the maximum distance to the grid data points to be considered during filtering, should be small for computational reasons. Figure 3

displays the impulse responses of the different filters under investigation, where the filter widths are scaled so that all filters approximate an ideal low pass filter with the same cut-off frequency. Figure 3 shows that the rectangle filter works with the smallest number of data points during filtering, while the other filters need a considerably larger number of points. To compare the different filter designs, the corresponding passband characteristics $U(\nu) = |G(\nu)|^2$ were calculated. The passband characteristics show that all filter designs have a very similar passband droop. None of the filters displays a sharp cut-off in the frequency domain, which would be the ideal case. Analyzing in Figure 4 the pass band ripple, the rectangle filter displays a strong oscillation, leaving relatively high energy in the high frequency bandwidths. A similar behaviour is displayed for the triangle filter, although the amplitudes are largely reduced. The Gauss filter does not produce such oscillations, but is approaching zero quite slowly, leaving significant energy at frequencies that are three to four times the cut-off frequency. The Hanning window has a transfer function similar to the triangle filter up to about four times the cut-off frequency but then picks up significantly less power for higher frequencies. The best results can be obtained using the Hamming filter, the first minimum will be reached at a slightly higher frequency than with the Hanning filter, but the higher frequency oscillations are less pronounced. The Hamming filter therefore is applied in the following for filtering the geoid and sea surface height models.

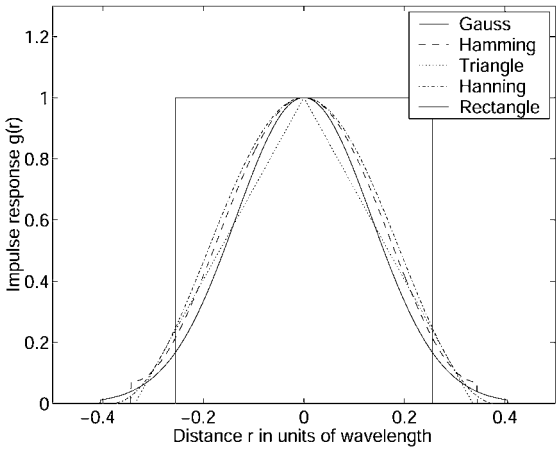

Figure 3. Impulse responses of different filters for low-pass filtering in the spatial domain. The distances are given in units of the cut-off wavelength to make the filter properties comparable.

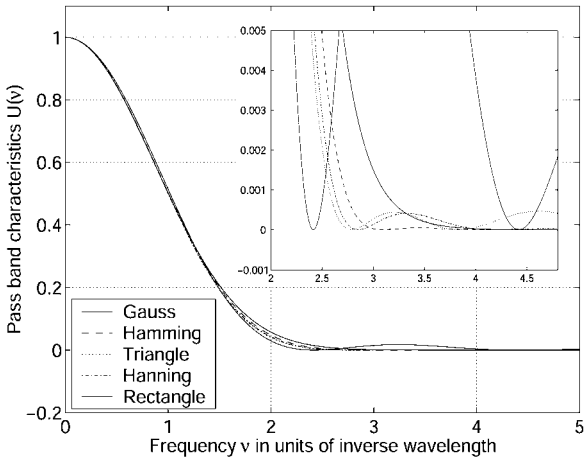

Figure 4. Passband characteristics of different low pass filters as a function of inverse cut-off wavelength i.e., that wavelength where the amplitude of the signal is damped by factor 0.5.

To compare filtering on the sphere in the spatial domain with a simple truncation at a certain degree l of a spherical harmonic expansion, it is necessary to relate the cut-off wavelength $\lambda=\nu^{-1}$ to the truncation degree l [Cazenave and Royer, 2001]:

$$\lambda \approx \frac{2\pi R}{\sqrt{l(1+l)}} \tag{2}$$

with R being the mean Earth radius.

Equation (2) allows to give the resulting resolution of the filtered fields as well in units of spatial wavelength as in degrees of a spherical harmonic expansion. Table 2 illustrates for the two examples being relevant here, the relations between cut-off wavelength, truncation degree and the range of the spherical distance to the grid points contributing to one filtered value.

Table 2. Relation between cut-off wavelength, spherical harmonic truncation degree and maximum spherical distance to input data points using the Hamming filter.

Cut-off wavelength λ	Spher. harm. truncation degree l	Maximum spherical distance r
1000 km	40	344 km
1800 km	22	619 km

5 *Sea Surface Topography*

The geoid is defined as the equipotential surface of the gravitational field that coincides with the undisturbed ocean. This ocean will be in a state of equilibrium, subject only to the force of gravity, and free from variations with time [Torge, 2001]. The deviation of the stationary sea surface height H from the geoid undulation N (both related to the same conventional ellipsoid of revolution) is called the sea surface topography ζ:

$$\zeta = H - N \tag{3}$$

An estimation $\hat{\zeta}$ of the sea surface topography then is simply obtained from the difference between the appropriately filtered models of the MSSH and the geoid. The values were calculated on a regular grid with 1 deg spacing.

In order to be able to separate sea surface topography signals from high frequency errors, some qualitative a priori information about the sea surface topography must be known. This information is used to determine the optimum cut-off wavelength of the low pass filter to be applied to both data fields. Sea surface topography estimated from oceanographic in-situ measurements of temperature and salinity has been published by Levitus [Levitus, 1982]. Global ocean circulation models provide additional information, like the Parallel Ocean Climate Model [Semtner and Chervin, 1992] or the Hamburg Ocean Model for Circulation and Tides [Thomas et al., 2001]. The sea surface topography is dominated by long wavelength features. High gradients are expected only in the western boundary current regions. In general, zonally aligned structures predominate.

For the EIGEN-2 gravity field the optimum resolution was found to be at the cut-off wavelength of 1800 km. This corresponds to a spherical harmonic expansion up to degree l = 22. Looking at Figure 5, there is some high frequency noise left. Nevertheless, the typical features of the large scale surface circulation are well pronounced, like the northern Pacific gyre with steepest gradients in the Kuroshio region. A similar but attenuated pattern can be seen in the northern Atlantic with the Gulf Stream off North America. The circulation cells in the southern Pacific and Atlantic are generally weaker, in accordance with the a priori information. The existence of a circulation system in the Indic ocean east of Madagascar is evident.

Analysing the sea surface topography model using the EIGEN-GRACE01S gravity field model (Figure 6), a cut-off wavelength of 1000km (or degree l = 40 in terms of spherical harmonics) was found to be the optimal choice in order to preserve most of the oceanic signal.

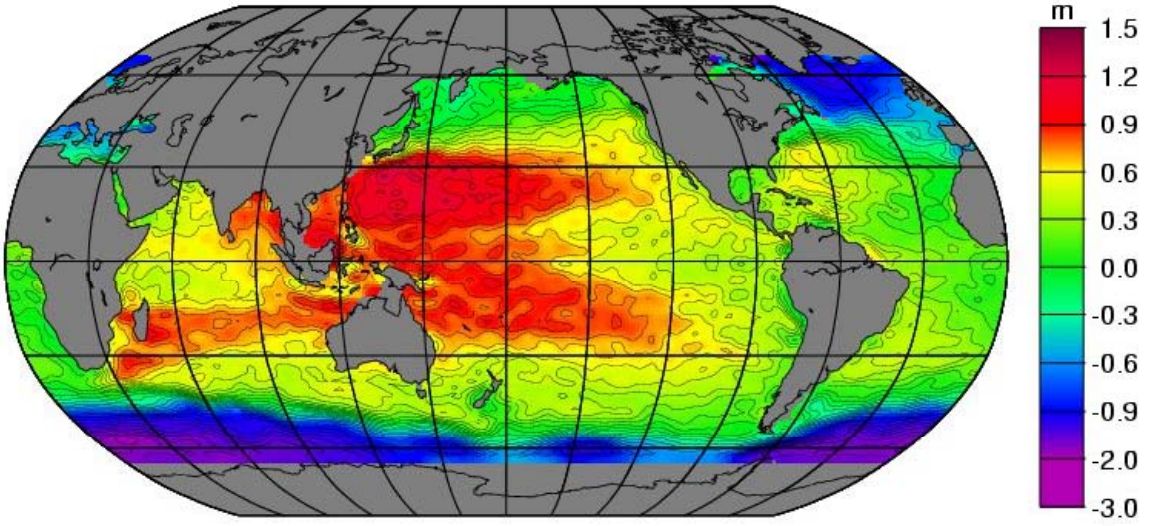

Figure 5. Sea surface topography [m] derived from TOPEX altimetric mean sea surface height model and the CHAMP geoid model EIGEN-2, both low-pass filtered by a Hamming filter with a cut-off wavelength of 1800 km.

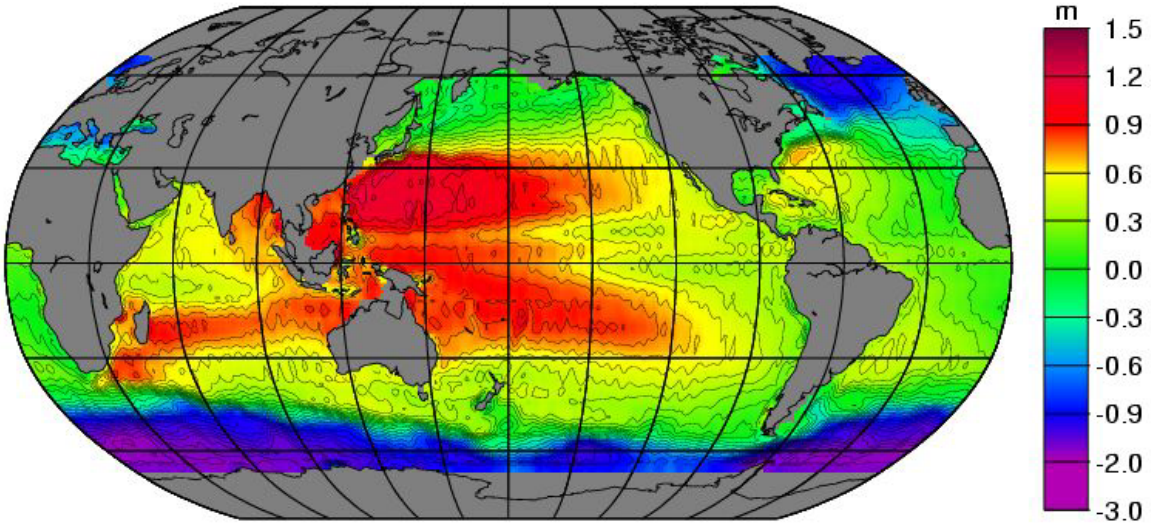

Figure 6. Same as Figure 4 but using the GRACE geoid model EIGEN-GRACE01S and a at cut-off wavelength of 1000 km.

The large scale circulation systems are now clearly defined. In some regions a significant north-south aligned pattern can be realised, e.g. in the north Pacific or the Indian ocean west of Australia. These signals are due to unresolved systematic errors in this first GRACE gravity field solution.

According to Figure 2, the geoid accuracy of EIGEN-2 is estimated to be about 2 cm at 1800 km (l = 22) wavelength which is also confirmed by the difference geoid amplitudes between the CHAMP and GRACE models. The value of 2 cm can be considered as the upper limit for the geoid accuracy when used in sea surface topography recovery.

The limitations with the EIGEN-GRACE01S model (cut-off wavelength 1000 km) are due to the increasing erroneous stripe-like features, increasing with increasing resolution, rather than to the estimated noise (Figure 2). Nevertheless, evaluating only 39 days of GRACE data almost doubles the resolution compared to the CHAMP model.

6 Geostrophic Surface Currents

The motion of a fluid can be generally described by the Navier-Stokes equation combining the effects of pressure gradient, internal friction, gravity gradient and the Coriolis-force originating from the rotation of the Earth. Apart from the coastal and equatorial regions, and for periods longer than a few days the pressure gradient and the Coriolis-force dominate all other accelerating forces that then can be neglected [Pond and Pickard, 1983]. The resulting relation between the pressure gradient and the Coriolis-force is called the geostrophic balance and can be written as [Wunsch, 1993]:

$$\begin{aligned} 2\omega \sin\varphi \cdot u &= \frac{-g}{R} \cdot \frac{\partial \zeta}{\partial \varphi} \quad , \\ 2\omega \sin\varphi \cdot v &= \frac{g}{R \cdot \cos\varphi} \cdot \frac{\partial \zeta}{\partial \lambda} \quad , \end{aligned} \tag{4}$$

with u and v being the geostrophic velocity at the surface in east-west and north-south direction, respectively, g the gravitational acceleration, R the Earth's equatorial radius, φ latitude, λ longitude and ω angular velocity of Earth's rotation.

Geostrophic balance is valid in the oceans at least at latitudes exceeding roughly 3 deg north and south, and seems to be valid much closer to the equator [Wunsch and Stammer, 1998]. However, inspecting Equation (4), it is obvious that due to the singularity in Equation (4) at the equator and the unfavourable error propagation, geostrophic velocities close to the equator must not be interpreted. The geostrophic sea surface velocities resulting from the CHAMP and GRACE sea surface topography models and applying Equation (4) are shown in Figure 7 and 8, respectively.

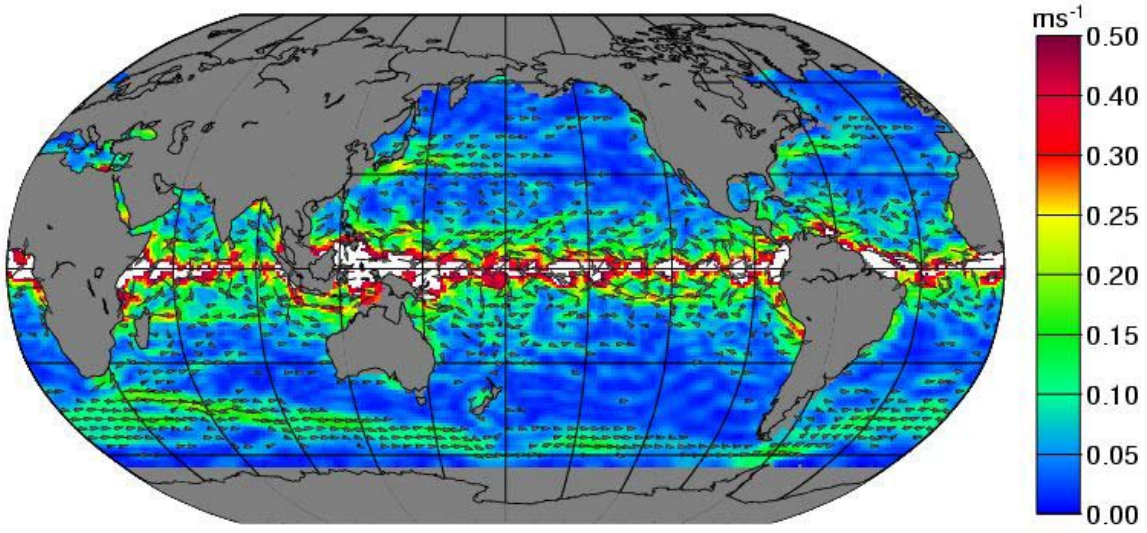

Figure 7. Geostrophic sea surface velocities [m/s] derived from CHAMP EIGEN-2 sea surface topography shown in Figure 5. Arrows, indicating the direction of the currents, have been omitted when the velocities are smaller than 5 cm/s. Since the geostrophic approximation is not valid in the vicinity of the equator, velocities have not been calculated up to 0.5 degrees off the equator.

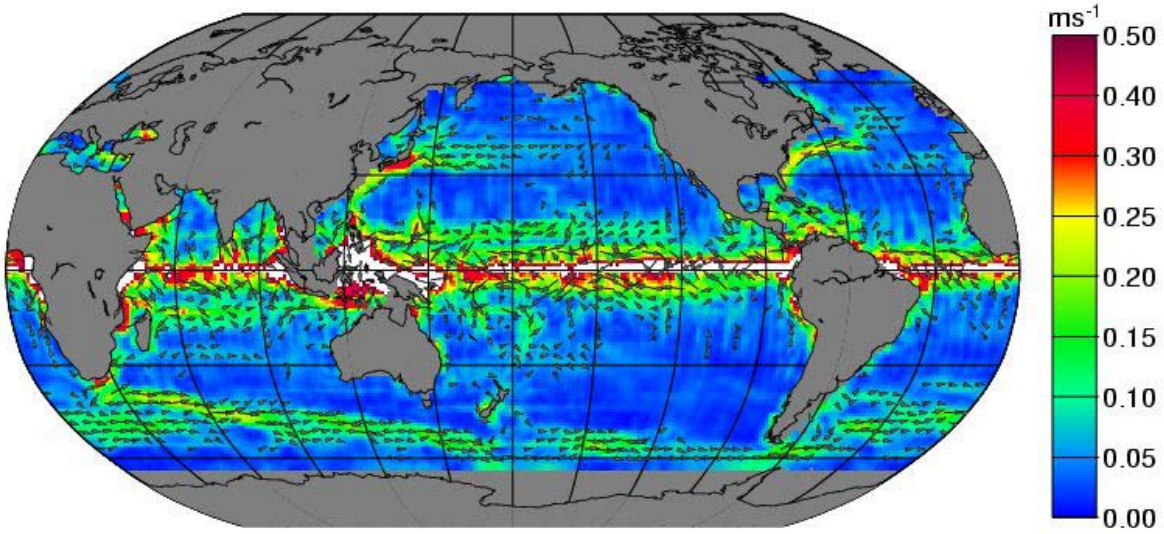

Figure 8. Same as Figure 7 but using the EIGEN-GRACE01S sea surface topography (Figure 6) to derive the geostrophic sea surface velocities.

The standard deviations of the estimated surface velocity components as a function of the geoid models' accuracy are estimated using Equation (4) for an error propagation:

$$s_u = \frac{g}{2\omega \sin\varphi} \cdot s_\varsigma$$
$$s_v = \frac{g}{2\omega \sin\varphi} \cdot s_\eta \quad . \tag{5}$$

It turns out that the standard deviations s_u and s_v of the velocity components u and v are proportional to s_ξ and s_η of the geoid's horizontal gradients

$$\xi = -\frac{1}{R} \cdot \frac{\partial N}{\partial \varphi}$$

in north-south direction and (6)

$$\eta = -\frac{1}{\mathrm{R}\cos\varphi} \cdot \frac{\partial \mathrm{N}}{\partial \lambda}$$

in east-west direction, respectively.

Given the variance-covariance matrices of the spherical harmonic coefficients of the EIGEN-2 and EIGEN-GRACE01S gravity field models and expressing ξ and η in terms of spherical harmonics, a rigorous error propagation is performed to get the geographical distribution of the geoid induced standard deviations s_u and s_v. In accordance with the sea surface topography resolution limits found above, the variances and covariances of the coefficients up to degree/order 22 in the case of the CHAMP model and up to degree/order 40 in the case of the GRACE model were propagated.

Table 3 gives the resulting geoids' error contribution (noise only) to the surface velocity estimations as depicted in Figures 7 and 8. The errors are principally a function of latitude increasing towards the equator. The requirement postulated by Martel and Wunsch [1994] for an ocean current velocity recovery precision of better than 10 mm/s, using geodetic methods, is well achieved (with the exception of low latitude zones in the case of the CHAMP geoid) for the spectral wavelengths up to l = 22 and l = 40 covered by the EIGEN-2 and EIGEN-GRACE01S geoid models, respectively. Taking into account that the noise level induced by the GRACE geoid is much lower than the threshold of 10 mm/s again indicates that the systematic north-south aligned geoid errors are the limiting resolution factor rather than the noise. The coming GRACE gravity field solutions may solve this problem, then allowing on even higher resolution of the sea surface topography.

Table 3. Geoid induced error contribution (noise) to geostrophic surface velocity estimates.

Latitude	**EIGEN-2 (l_{max} = 22)**		**EIGEN-GRACE01S (l_{max} = 40)**	
$\|\varphi\|$ [deg]	s_u [mm/s]	s_v [mm/s]	s_u [mm/s]	s_v [mm/s]
75	2.2	1.7	0.1	0.1
45	3.6	1.9	0.3	0.3
20	7.9	2.5	0.8	1.2
10	15.6	4.9	1.5	2.3

The estimated 2 cm accuracy in the MSSH model induces another error component in surface velocity recovery. Taking into account that the relative velocity error is proportional to the relative error in the horizontal gradient of the sea surface topography model and assuming an average gradient of 1 m over 500 km half-wavelength, the 2 cm elevation error introduces a 2 % error in the surface velocity estimations, on average. This already exceeds the noise level coming from the GRACE geoid (c.f. Table 3). Therefore, striving for higher resolutions in geostrophic velocity recovery, the MSSH model accuracy will be the limiting factor rather than the geoid model accuracy as pointed out already in Tapley et al. [2003].

The geostrophic surface currents based on EIGEN-2 (Figure 7), show very high and irregular velocity currents in the equatorial region which should not be interpreted as stated above. The major current systems can be detected: Current velocities of 25 cm/s are evident in the Kuroshio region southeast off Japan. The Gulf stream is leaving the American coast east off Cape Hatteras progressing towards the Labradorean Sea and northern Europe with top velocities around 15 cm/s. In the central North Atlantic there are indications for a closing of the circulation cell with Canary stream and the North Equatorial current. In the South Atlantic there are some slight evidences for the Brazil current flowing southward along the coast, and the Falkland current emerging from the Drake Passage together with the Antarctic Circumpolar Current (ACC). Concerning the ACC, a very clear northwards extension in the Atlantic and the Indian Ocean can be recognised, while crossing the southern Pacific, the ACC is significantly depressed southwards due to the stream boundaries of New Zealand and the Drake Passage. The high current velocities along the western South American coast are probably caused by locally high geoid gradients which were smoothed out during filtering. In the Indian ocean the flow pattern of the southern Equatorial Current east of Madagascar is visible as well as some evidences for the Agulhas current south of Cape Hope.

Geostrophic velocities based on EIGEN-GRACE01S are displayed in Figure 8. In general, the global pattern of ocean currents becomes clearer due to the higher resolution. Apparent flows along the west coast of South America and the Tonga-Kermaduec-Trench are again induced by the lack of high-frequency features in the filtered satellite gravity field model. The western boundary current regions are well defined with highest velocities of 40 cm/s south off Japan in the Kuroshio region. The estimated velocities in the Gulf Stream region are with a maximum amplitude of about 25 cm/s significantly weaker, but clearly visible. The Brazil and Falkland currents in the South Atlantic are resolved. A clockwise circulation in the Pacific around New Zealand can be recognised. Keeping in mind the existence of an anticlockwise rotating Kelvin wave generated by tidal forces, it remains open, whether this pattern originates from an oceanic circulation mechanism or from a mismodelling in the tidal models used in the generation of the sea surface height model.

In the Indian ocean the Agulhas area shows current velocities up to 30 cm/s. West of Madagascar there is a broad zonally aligned band of the South Equatorial current with velocities of 10 to 15cm/s. A similar feature can be resolved in the northern subtropical Pacific, known as the North Equatorial current.

7 Conclusions

With the new dedicated gravity missions CHAMP and GRACE, the accuracy of satellite-only long-to-medium wavelength marine geoid models has reached the level 1 to 2 cm, so that the sea surface topography can be reliably observed from space with a resolution down to 1800 km (CHAMP) and 1000 km (GRACE) by relating an altimetric mean sea surface height model to a satellite-based marine geoid. The Hamming filter was found to be adequate for low pass filtering of the sea surface heights and geoid models in order to damp poorly determined high frequency signals, which otherwise would mask the sea surface topography and prohibit the estimation of geostrophic velocities. The resolution limit of 1800 km for the CHAMP derived EIGEN-2 model is caused by the geoid's accuracy that exceeds the 2 cm-level for higher resolutions. The solution is almost doubled to 1000 km using the first GRACE geoid derived from only 39 days of mission data. Still unresolved systematic errors in this model prevent a further increase in resolution rather than the noise level. The derived geostrophic sea surface velocities display very well the major ocean current systems with higher amplitudes for the higher resolving GRACE-based solution.

Further improvements can be expected with the coming GRACE global gravity models when the data processing will be improved and a longer data period will be exploited.
Simulation studies for the European GOCE gravity gradiometer mission indicate that a 1 cm geoid accuracy at 200 km wavelength can be achieved [Le Provost and Bremond, 2003] to meet the demanding oceanographic needs in global ocean circulation recovery from space.
Additionally attempts are made to combine geodetic measurements of sea surface topography and dynamic ocean circulation models using inverse modelling techniques [Le Grand et al., 2003], which will also benefit from the new generation of dedicated satellite gravity missions.
For a complete general ocean circulation description the knowledge of the three-dimensional density distribution is required. There are currently different approaches to assimilate the absolute geostrophic surface velocities into numerical oceanic models in order to calculate the currents at depth and estimate heat and mass transports in the oceans, which have a major impact on the Earth's climate evolutions [Le Traon et al., 2003], [Wunsch and Stammer, 2003].

Acknowledgement

The German Ministry of Education and Research (BMBF) supports the CHAMP and GRACE project within the GEOTECHNOLOGIEN geoscientific R + D programme under grant 50EP9587 and 03F0326A, respectively.

References

C. Wunsch, E.M. Gaposchkin, On Using Satellite Altimetry to Determine the General Circulation of the Oceans With Application to Geoid Improvement, Rev. Geophys. Space Phys. 18, 725-745 (1980)

C. Wunsch, D. Stammer, Satellite Altimetry, the marine geoid and the oceanic general circulation, Annu. Rev. Earth Planet. Sci. 26, 219-253 (1998)

L.-L. Fu, D.B. Chelton, Large-scale ocean circulation, in: L.-L. Fu, A. Cazenave (Eds.), Satellite Altimetry and Earth Sciences, University Press, Cambridge, 133-169 (2001)

P.Y. Le Traon, P. Schaeffer, S. Guinehut, M.H. Rio, F. Hernandez, G. Larnicol, J.M. Lemoine, Mean Ocean Dynamic Topography from GOCE and Altimetry, Int. GOCE Workshop, Noordwijk (2001)

Ch. Reigber, P. Schwintzer, K.-H. Neumayer, F. Barthelmes, R. König, Ch. Förste, G. Balmino, R. Biancale, J.-M. Lemoine, S. Loyer, S. Bruinsma, F. Perosanz, T. Fayard, The CHAMP-only Earth Gravity Field Model EIGEN-2, Adv. Space Res. 31, 1883-1888 (2003a)

Ch. Reigber, R. Schmidt, F. Flechtner, R. König, U. Meyer, K.-H. Neumayer, P. Schwintzer, S.Y. Zhu, First GFZ GRACE gravity field model EIGEN-GRACE01S, http://op.gfz-potsdam.de/grace/results (2003b)

Th. Gruber, P. Steigenberger, Impact of new Gravity Field Missions for Sea Surface Topography determination, in: I.N. Tziavos (Ed.), Gravity and Geoid, 3rd Meeting of the International Gravity and Geoid Commission (IGGC), Univ. Of Thessaloniki, Greece, 320-325 (2002)

B.D. Tapley, D.P. Chambers, S. Bettadpur, J.C. Ries, Large scale ocean circulation from the GRACE GGM01 Geoid, Geophys. Res. Let. 30(22), 10.1029/2003GL018622 (2003)

F. Hernandez, P. Schaeffer, The CLS01 Mean Sea Surface: A validation with the GSFC00 surface. in press, CLS Ramonville St Agne, France (2001)

Y.M. Wang, GSFC00 mean sea surface, gravity anomaly, and vertical gravity gradient from satellite altimeter data J. Geophys. Res. 106 (C12), 31167-31174 (2001)

Ch. Reigber, G. Balmino, P. Schwintzer, R. Biancale, A. Bode, J.-M. Lemoine, R. König, S. Loyer, K.-H. Neumayer, J.-C. Marty, F. Barthelmes, F. Perosanz, S.Y. Shu, A high-quality global gravity field model from CHAMP GPS tracking data and accelerometry (EIGEN-1S), Geophys. Res. Lett. 29 (14), 10.1029/2002GL015064 (2002)

NASA, TOPEX/POSEIDON: A United States/France mission, in: Oceanography from space: The oceans and climate, National Aeronautics and Space Administration, Washington, DC., NASA-TM-108253 (1992),

R. Ray, A Global Ocean Tide Model from TOPEX/POSEIDON Altimetry: GOT99.2, NASA Technical Memorandum, NASA/TM-1999-209478, National Aeronautics and Space Administration, Goddard Space Flight Center, Greenbelt, MD (1999)

D.E. Cartwright, R.J. Tayler, New computations of the tide-generating potential, Geophys. J. R. Astr. Soc. 23, 45-74 (1971)

D.E. Cartwright, A.C. Edden, Corrected tables of tidal harmonics, Geophys. J. R. Astr. Soc. 33, 253-264 (1973)

J.W. Wahr, Deformation of the Earth induced by polar motion, J. Geophys. Res. (Solid Earth) 90, 9363-9368 (1985)

R.H. Rapp, Y.M. Wang, N.K. Pavlis, The Ohio State 1991 Geopotential and Sea Surface Topography Harmonic Coefficient Models, Rpt. 410, Dept. of Geodetic Science and Surveying, The Ohio State University, Columbus (1991)

F. Hernandez, P. Schaffer, Altimetric mean sea surfaces and gravity anomaly maps inter-comparisons. AVISO Tech. Rep. AVI-NT-011-5242-CLS, Cent. Natl. d'Etudes Spatiales, Toulouse, France (2000)

D.B. Chelton, J.C. Ries, B.J. Haines, L.-L. Fu, P.S. Callahan, Satellite Altimetry, in: L.-L. Fu, A. Cazenave (Eds.) Satellite Altimetry and Earth Sciences, University Press, Cambridge, 1-131 (2001)

J.C. Ries, B.D. Tapley, Centimeter level orbit determination for the TOPEX/POSEIDON altimeter satellite. Adv. Astronomical Sci. 102, 583-598 (1999)

UTEX/CSR, http://www.csr.utexas.edu/grace/gravity (2003)

F.G. Lemoine, S.C. Kenyon, J.K. Factor, R.G. Trimmer, N.K. Pavlis, D.S. Chinn, C.M. Cox, S.M. Klosko, S.B. Luthcke, M.H. Torrence, Y.M. Wang, R.G. Williamson, E.C. Pavlis, R.H. Rapp, T.R. Olson, The development of the joint NASA GSFC and the National Imagery and Mapping Agency (NIMA) geopotential model EGM96. NASA Technical Paper NASA/TP-1998-206861, Goddard Space Flight Center, Greenbelt (1998)

R.H. Rapp, C. Zhang, Y. Yi, Analysis of dynamic ocean topography using TOPEX data and orthonormal functions, J. Geophys. Res. 101, C10 22583-22598 (1996)

A. Cazenave, J.Y. Royer, Applications to marine geophysics, in: L.-L. Fu, A. Cazenave (Eds.) Satellite Altimetry and Earth Sciences, University Press, Cambridge, 407-439 (2001)

W. Torge, Geodesy, de Gryter, Berlin (2001)

S. Levitus, Climatological Atlas of the World's oceans. NOAA Professional Paper, 18, U.S. Govt. Print. Off., Washington, D. C. (1982)

A.J. Semtner, R.M. Chervin, Ocean General Circulation from a Global Eddy-Resolving Model, J. Geophys. Res. 97, C4, 5493-5550 (1992)

M. Thomas, J. Sündermann, E. Maier-Reimer, Consideration of ocean tides in an OGCM and impacts on subseasonal to decadal polar motion excitation, Geophys. Res. Lett. 28(12), 2457-2460 (2001)

S. Pond, G.L. Pickard, Introductory Dynamical Oceanography, Pergamon Press, Oxford, (1983)

C. Wunsch, Physics of the ocean circulation, in: R. Rummel, F. Sanso (Eds.) Satellite Altimetry in Geodesy and Oceanography, Springer, Berlin, 9-98 (1993)

F. Martel, C. Wunsch, Combined Inversion of Hydrography, Current Meter Data and Altimetric Elevations for the North Atlantic Circulation, manuscripta geodaetica 18, 219-226 (1994)

C. Le Provost, M. Bremond, Resolution needed for an adequate Determination of the mean ocean circulation from Altimetry and improved Geoids, in: G. Beutler, M.R. Drinkwater, R. Rummel, R. Von Steiger (eds.) Earth Gravity Field from Space: From Sensors to Earth Sciences: Proceedings of an ISSI Workshop, 11-15 March 2002, Bern, Switzerland, Space Science Reviews 108 (1-2), 163-178 (2003)

P. LeGrand, E. J. O. Schrama, J. Tournadre, An inverse estimate of the dynamic topography of the ocean, Geophys. Res. Lett. 30(2), 10.1029/2002GL014917 (2003)

P. Y. Le Traon, F. Hernandez, M. H. Rio, F. Davidson, How operational oceanography can benefit from dynamic topography estimates as derived from altimetry and improved geoid?, in: G. Beutler, M.R. Drinkwater, R. Rummel, R. Von Steiger (eds.) Earth Gravity Field from Space: From Sensors to Earth Sciences: Proceedings of an ISSI Workshop, 11-15 March 2002, Bern, Switzerland, Space Science Reviews 108 (1-2), 239-249 (2003)

C. Wunsch, D. Stammer, Global Ocean Data Assimilation and Geoid Measurements, in: G. Beutler, M.R. Drinkwater, R. Rummel, R. Von Steiger (eds.) Earth Gravity Field from Space: From Sensors to Earth Sciences: Proceedings of an ISSI Workshop, 11-15 March 2002, Bern, Switzerland, Space Science Reviews 108 (1-2), 147-162 (2003)